



Universiteit
Leiden
The Netherlands

SDHD-related head and neck paragangliomas & their natural course

Heesterman, B.L.

Citation

Heesterman, B. L. (2018, September 13). *SDHD-related head and neck paragangliomas & their natural course*. Retrieved from <https://hdl.handle.net/1887/65453>

Version: Not Applicable (or Unknown)

License: [Licence agreement concerning inclusion of doctoral thesis in the Institutional Repository of the University of Leiden](#)

Downloaded from: <https://hdl.handle.net/1887/65453>

Note: To cite this publication please use the final published version (if applicable).

Cover Page



Universiteit Leiden



The handle <http://hdl.handle.net/1887/65453> holds various files of this Leiden University dissertation.

Author: Heesterman, B.L.

Title: SDHD-related head and neck paragangliomas & their natural course

Issue Date: 2018-09-13

Berdine L Heesterman, John-Melle Bokhorst, Lisa M H de Pont, Berit M Verbist, Jean-Pierre Bayley, Andel G L van der Mey, Eleonora P M Corssmit, Frederik J Hes, Peter Paul G van Benthem and Jeroen C Jansen

Journal of Neurological Surgery Part B: Skull Base, 2018

5

Mathematical models for tumor growth and the reduction of overtreatment

ABSTRACT

Background: To improve our understanding of the natural course of head and neck paragangliomas and ultimately differentiate between cases that benefit from early treatment and those that are best left untreated, we studied the growth dynamics of 47 carotid and 30 vagal body paragangliomas managed with primary observation.

Methods: Using digitally available MR Images, tumor volume was estimated at three time points. Subsequently, nonlinear least squares regression was used to fit seven mathematical models to the observed growth data. Goodness of fit was assessed with the coefficient of determination (R^2) and root mean squared error (RMSE). The models were compared with Kruskal-Wallis one-way analysis of variance and subsequent post-hoc tests. In addition, the credibility of predictions (age at onset of neoplastic growth and estimated volume at age 90) were evaluated.

Results: Equations generating sigmoidal-shaped growth curves (Gompertz, logistic, Spratt and Bertalanffy) provided a good fit (median R^2 of 0.996 - 1.00) and better described the observed data compared with the linear, exponential, and Mendelsohn equations ($p < 0.001$). Although there was no statistically significant difference between the sigmoidal-shaped growth curves regarding the goodness of fit, a realistic age at onset and estimated volume at age 90 were most often predicted by the Bertalanffy model.

Conclusions: Growth of head and neck paragangliomas is best described by decelerating tumor growth laws, with a preference for the Bertalanffy model. To the best of our knowledge, this is the first time that this often-neglected model has been successfully fitted to clinically obtained growth data.

INTRODUCTION

Head and neck paragangliomas (HNPGs) are generally benign tumors that arise from nonchromaffin paraganglion cells associated with the autonomic nervous system. They are most commonly located at the bifurcation of the carotid artery, but also occur at the nodose and jugular ganglion of the vagus nerve, and within the temporal bone, where they arise at the adventitia of the jugular bulb and along Arnold's and Jacobson's nerve. Head and neck paragangliomas at other locations, including the thyroid gland and larynx, are extremely rare [1–3].

Paragangliomas are associated with germline mutations in numerous genes, but mutations in *SDHD* are currently the most common cause of hereditary paragangliomas [4, 5]. An increasing number of paragangliomas are detected following surveillance in subjects with a genetic predisposition [6]. These “screening detected” paragangliomas are usually small and asymptomatic. However, as tumors become larger, symptoms related to compression and destruction of adjacent structures, including lower cranial nerve paralysis, may occur.

The risk of postoperative cranial nerve dysfunction and other serious complications, including stroke and aspiration/pneumonia, is relatively low following surgery for small carotid body tumors (8.3-26.7%) but increases to around 80% when the internal and external carotid arteries are completely encased by tumor tissue [7]. With this in mind, one could argue that all small carotid body tumors should be surgically resected. However, although tumor progression is, with long follow-up, observed in most HNPG, progression is generally slow and tumors may remain asymptomatic throughout life [8–10]. Thus, even though surgery for small carotid body tumors is reasonably safe, it remains uncertain whether the benefits outweigh the potential harm caused by treatment. Ideally, we would be able to differentiate between tumors that will never cause symptoms, and those that can best be treated while still small.

A better understanding of the natural course of tumors is vital to determine optimal screening intervals, model treatment response, and prevent overtreatment. Unsurprisingly, tumor growth laws have been of interest for over a century, and a variety of mathematical models have been proposed. As most tumors are treated shortly after diagnosis, tumor growth is primarily studied using mouse models or *in vitro* experiments [11–13].

We studied growth of HNPGLs using sequential MR imaging obtained during routine patient care. We previously observed a decreasing growth probability with increasing age and tumor volume, consistent with a decelerating growth pattern [9]. We, therefore, propose that a sigmoidal-shaped growth curve will best describe the growth of HNPGLs.

METHODS

SUBJECTS

SDHD mutation carriers were identified as previously described [9]. MRI scans were digitally available from 2002 onwards and sufficient follow-up was required to study growth patterns. To avoid selection of an atypically favorable subset of untreated tumors (i.e., tumors that were left untreated while already under surveillance), only patients diagnosed with HNPGL between January 2002 and 2009 were eligible for inclusion. For reasons earlier described, only carotid and vagal body paragangliomas were included [9]. In addition, a minimum of three consecutive MRI scans, before any intervention, was deemed a prerequisite for inclusion. In accordance with the Dutch law, approval of the institutional ethics committee was not obtained because all data were collected in the course of routine patient care.

VOLUME ESTIMATION

Three perpendicular dimensions were measured using a linear digital caliper tool, at three different time points. Tumor volume was subsequently calculated, assuming an ellipsoid shape (5.1). Measurements were performed by two observers (BLH and LMHP) and executed as described in our earlier work on growth of HNPGL [9, 14].

$$Volume(V) = \frac{4}{3}\pi\left(\frac{1}{2}A * \frac{1}{2}B * \frac{1}{2}C\right) \quad (5.1)$$

MATHEMATICAL MODELS

Seven mathematical models of tumor growth were investigated (figure 5.0.1 on page 96).

LINEAR MODEL

The simplest model to describe the increase in tumor volume (V) over time (t) is linear growth, with a constant growth rate (r) independent of tumor size.

$$V(t) = V_0 + rt \quad (5.2)$$

EXPONENTIAL MODEL

If all tumor cells are proliferating at a constant rate, tumor volume increases exponentially. Relative growth rate and thus tumor doubling time (T_d) remain constant over time [11, 12, 15].

$$V(t) = V_0 e^{rt} \quad (5.3)$$

$$T_d = \frac{\ln 2}{r} \quad (5.4)$$

MENDELSON MODEL

Although tumor doubling is probably constant during early tumor growth, T_d eventually increases. An adjustment to exponential growth was therefore proposed by Mendelsohn in 1963. If $a = \frac{2}{3}$, growth is proportional to the surface area of the tumor, consistent with linear growth of tumor diameter [11, 12].

$$V(t) = (V_0^{1-a} + (1-a)rt)^{\frac{1}{1-a}} \quad (5.5)$$

GOMPertz MODEL

Perhaps the best-known tumor growth model, the Gompertz model was introduced in 1825 as a tool to determine the value of life insurance, and was first used by Anna Laird for the explanation of tumor growth [11, 16]. The inflection point of this sigmoid-shaped model occurs once 37% of the maximum tumor volume (V_∞) has been reached. Thereafter, the growth rate decreases exponentially.

$$V(t) = V_0 e^{\ln(V_\infty/V_0)(1-e^{-rt})} \quad (5.6)$$

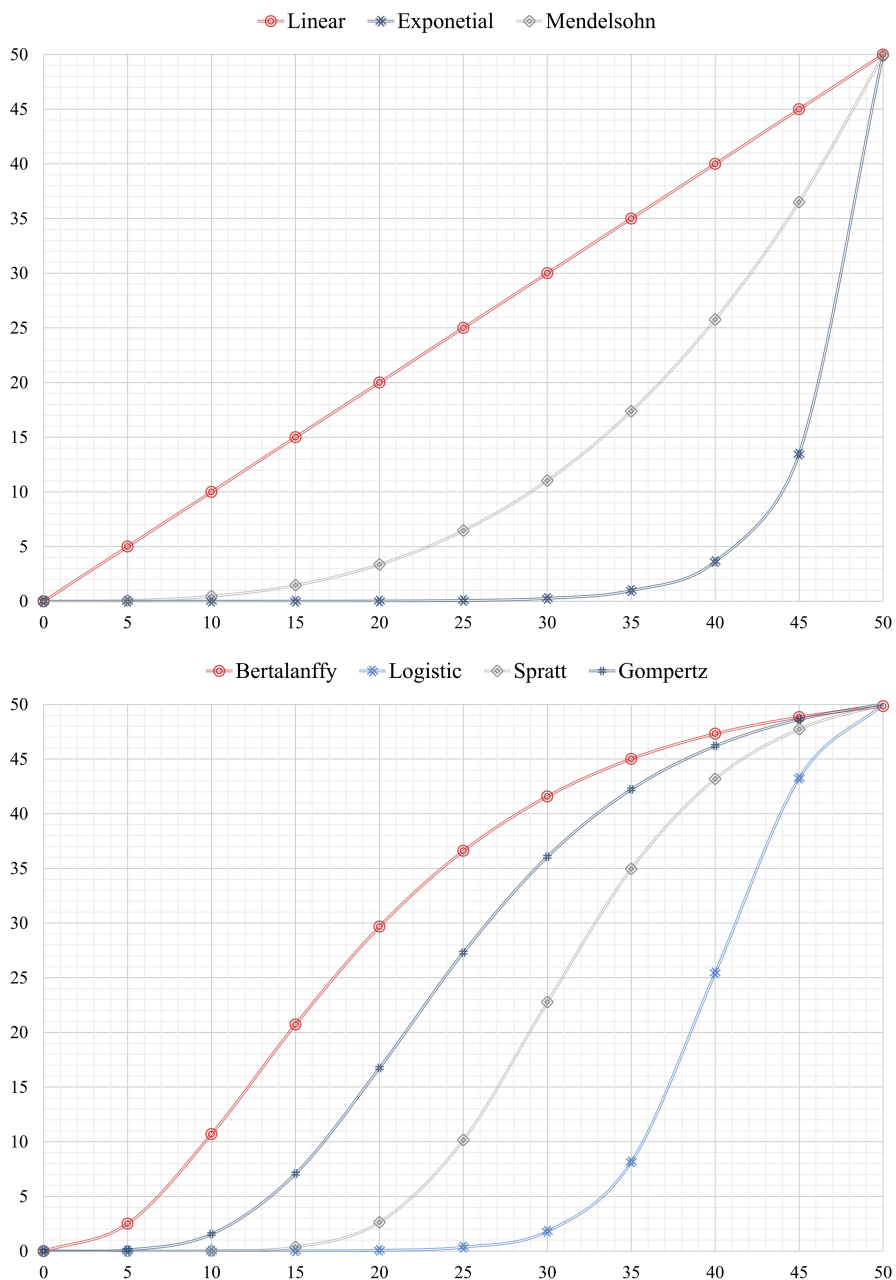


Figure 5.0.1: The investigated models could be subdivided in equations generating a sigmoidal-shaped growth curve (bottom panel) and those predicting ever-expanding tumor volume (upper panel).

LOGISTIC MODEL

The second model originating in the 19th century is the Logistic model, also sigmoidal in shape and first used to describe population dynamics. After 50% of the final size has been reached, growth rate decreases linearly with tumor size [11].

$$V(t) = V_{\infty} [1 + ((V_{\infty}/V_0) - 1)e^{-rt}]^{-1} \quad (5.7)$$

SPRATT MODEL

Spratt et al. found that a generalized logistic model with $\beta = \frac{1}{4}$ best described the growth of human breast cancer [17].

$$V(t) = V_{\infty} [1 + ((V_{\infty}/V_0)^{\frac{1}{4}} - 1)e^{-\frac{1}{4}rt}]^{-4} \quad (5.8)$$

BERTALANFFY MODEL

The final model we considered is the Bertalanffy model. This model is based on the assumption that growth results from a balance between cell proliferation and cell death. Proliferation occurs in proportion to the surface area ($\gamma = \frac{2}{3}$) and loss of tumor mass due to cell death is proportional to tumor volume (with constant β) [11, 13, 18]. Areas of necrosis are usually observed when head and neck paragangliomas become larger [19].

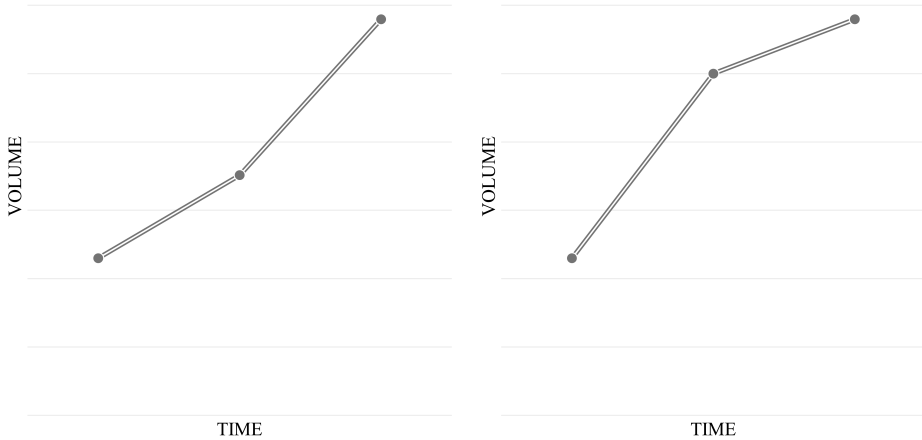
$$V(t) = \left(\frac{\alpha}{\beta} + (V_0^{1-\gamma} - \frac{\alpha}{\beta}) e^{-\beta(1-\gamma)t} \right)^{\frac{1}{1-\gamma}} \quad (5.9)$$

STATISTICS

The mathematical models were fitted using nonlinear least squares regression, with a convergence tolerance for parameters of 10^{-6} . Subsequently, the predicted age at onset of neoplastic growth and tumor volume at age 90 were calculated. Considering that the largest HNPGI we have encountered thus far had an estimated volume of 820 cm³ (patients age \approx 60 years), a volume of 1000 cm³ was regarded as the maximum realistic predicted volume at age 90. Goodness of fit statistics, including the coefficient of determination (R^2) and root mean squared error (RMSE) were used to compare the

different models. Kruskal-Wallis one-way analysis of variance, followed by post-hoc tests, was performed to determine statistical significance. Continuous data are, if normally distributed, expressed as mean \pm SD, otherwise the median and interquartile range (IQR) are provided. A p-value < 0.05 was considered statistically significant.

A: n = 42 (54.5%) & > SDD: 42 (100%) **B:** n = 20 (26.0%) & > SDD: 17 (85%)



C: n = 5 (6.5%) & > SDD: 4 (80%)

D: n = 10 (13%) & > SDD: 1 (10%)

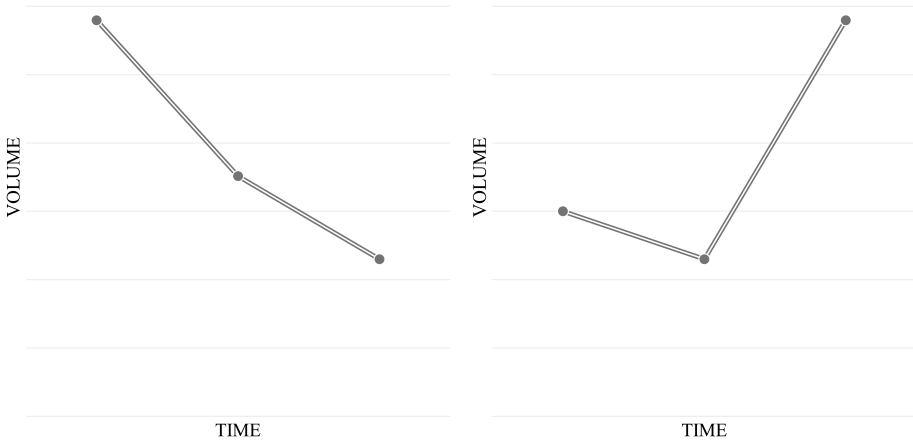


Figure 5.0.2: The observed growth patterns, accelerating (a) and decelerating (b) growth, gradual regression (c) and alternated progression and regression (d). The frequency and how often progression or regression exceeded the smallest detectable difference (SDD) are provided for each pattern.

RESULTS

SUBJECTS

Sequential MR imaging was obtained for 47 (61%) carotid body and 30 (39%) vagal body paragangliomas, managed with primary observation. These 77 HNPGL were diagnosed in 44 patients, with a mean age at baseline of 42 ± 12 years. Twenty-seven (61%) subjects were male and 91% carried the c.274G>T, p.Asp92Tyr Dutch founder mutation, while the remaining patients carried other known germline mutations in SDHD. Median tumor volume was 4.6 cm^3 at baseline and increased to 8.0 cm^3 during a mean observation period of 6.9 ± 2.0 years (range: 3.0-11.8). The cases presented here were also included in our previous work on growth of HNPGL [9].

OBSERVED GROWTH PATTERNS

Four growth patterns could be distinguished (figure 5.0.2). Gradual increase in tumor volume was observed in 62 cases (80.5%), and could be further subdivided in accelerating (figure 5.0.2a) and decelerating (figure 5.0.2b) growth. Spontaneous regression was observed in five cases (6.5%). In the remaining cases (13%) growth was characterized by alternating progression and regression (figure 5.0.2d). In 83%, progression or regression exceeded the previously determined smallest detectable difference (SDD) of 10% and 25% for carotid and vagal body tumors, respectively. Particularly when a gradual increase or decrease of tumor volume was observed, growth or regression exceeded the SDD.

MATHEMATICAL MODELS & GOODNESS OF FIT

The median R^2 , interquartile range and outliers are shown in figure 5.0.3 on the next page. A box and whisker diagram is also provided for the root mean squared error (figure 5.0.3). There was a statistically significant difference between the different mathematical models, with test statistic $H(6) = 80.23$ and $p < 0.001$. Focused comparisons of the mean ranks revealed that the sigmoidal-shaped growth curves (logistic, Spratt, Gompertz and Bertalanffy equation) better described the observed data compared with the linear, exponential, and Mendelsohn equations. Within the two groups (sigmoidal and nonsigmoidal-shaped growth curves) there was no statistically significant difference. An example of all models fitted to patient data is presented in figure 5.0.4 on page 103.

A realistic predicted age at onset (i.e., after conception) can, by the very nature of the proposed models, not be expected if the estimated volume is smaller at the end compared with the start of follow-up. Therefore, these cases ($n = 9$) were not included in further analysis. Dependent on the mathematical model fitted, the predicted age at onset was regarded as realistic in 28%-87% of cases, with the median age ranging from 13-34 years (table 5.0.1 on the next page). In the remaining cases, the estimated volume at birth was generally small (median: 0.32-1.46), although outliers were observed. Volume at age 90 was predicted to be less than 1000 cm³, in 41-96% of cases, with the median predicted volume ranging from 23.7-74.9 cm³. A realistic predicted age at onset and volume at age 90 were most often observed for the linear model, followed by the Bertalanffy model.

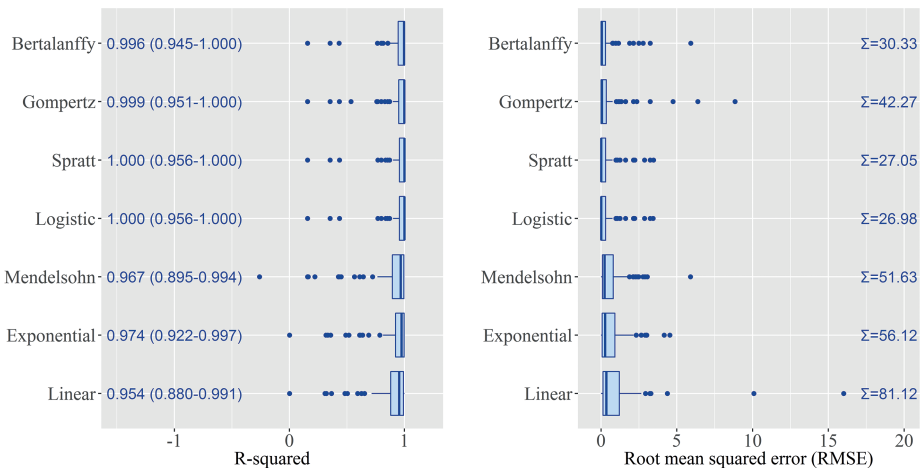


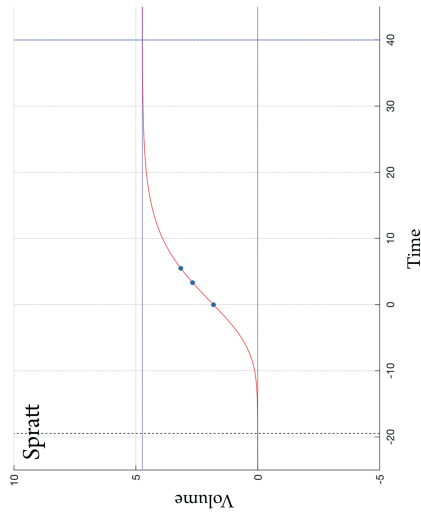
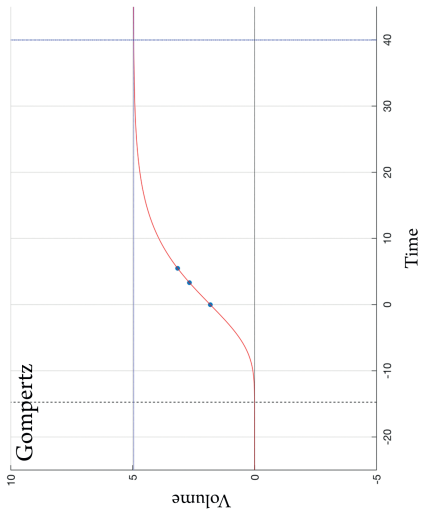
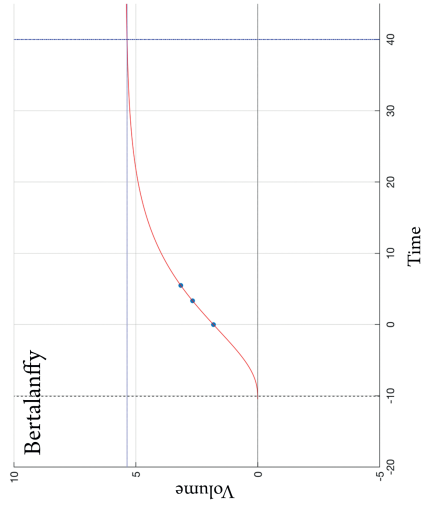
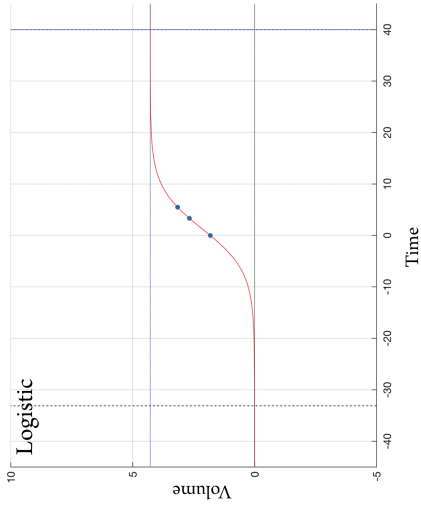
Figure 5.0.3: Box and whisker diagram for the R^2 (left panel) and root mean squared error (right panel). The median R^2 (IQR) is provided for all mathematical models, a value of $R^2 = 1$ indicates a perfect fit. For each model, the root mean squared error (RMSE) was summed for all patients, with the lowest value indicating the best fit. The lower whiskers (left panel) represent the smallest observed $R^2 \geq \text{first quartile } (Q_1) - 1.5 * \text{IQR}$ and the upper whiskers (right panel) represent the largest observed $\text{RMSE} \leq \text{third quartile } (Q_3) + 1.5 * \text{IQR}$. The blue dots represent the outliers.

Table 5.0.1: The number and proportion of cases with a realistic age at onset¹ and predicted volume at age 90² detailed for each model. Median age at onset and volume at age 90 are given for cases with realistic values. The 68 cases in which the tumor volume at the end of follow-up exceeded the initial volume were included in this table

	Number (%) or Median (IQR)						
	Linear	Exponential	Mendelsohn	Logistic	Spratt	Gompertz	Bertalanffy
Realistic ¹ age at onset	59 (87%)	19 (28%)	47 (69%)	44 (65%)	44 (65%)	50 (74%)	57 (84%)
Median age (years) at onset (if realistic ¹)	34 (23-43)	13 (3-18)	21 (13-31)	13 (7-23)	20 (12-30)	23 (14-32)	28 (21-36)
Volume (cm ³) at birth (if onset < conception)	1.46 (0.70-6.01)	0.33 (0.02-2.01)	0.81 (0.30-5.69)	0.37 (0.02-1.90)	0.32 (0.02-1.89)	0.82 (0.04-2.58)	0.76 (0.46-6.38)
Realistic ² volume at age 90	68 (100%)	41 (60%)	60 (88%)	57 (84%)	55 (81%)	60 (88%)	65 (96%)
Median volume (cm ³) at age 90 (if realistic ²)	32.5 (11.9-83.3)	74.9 (21.5-350.1)	63.7 (27.6-143.3)	23.7 (8.0-58.5)	25.0 (8.1-61.6)	31.1 (10.7-78.2)	35.7 (12.9-81.5)

Note 1: i.e., after conception (defined as 9 months before birth)

Note 2: i.e., if ≤ 1000 cm³



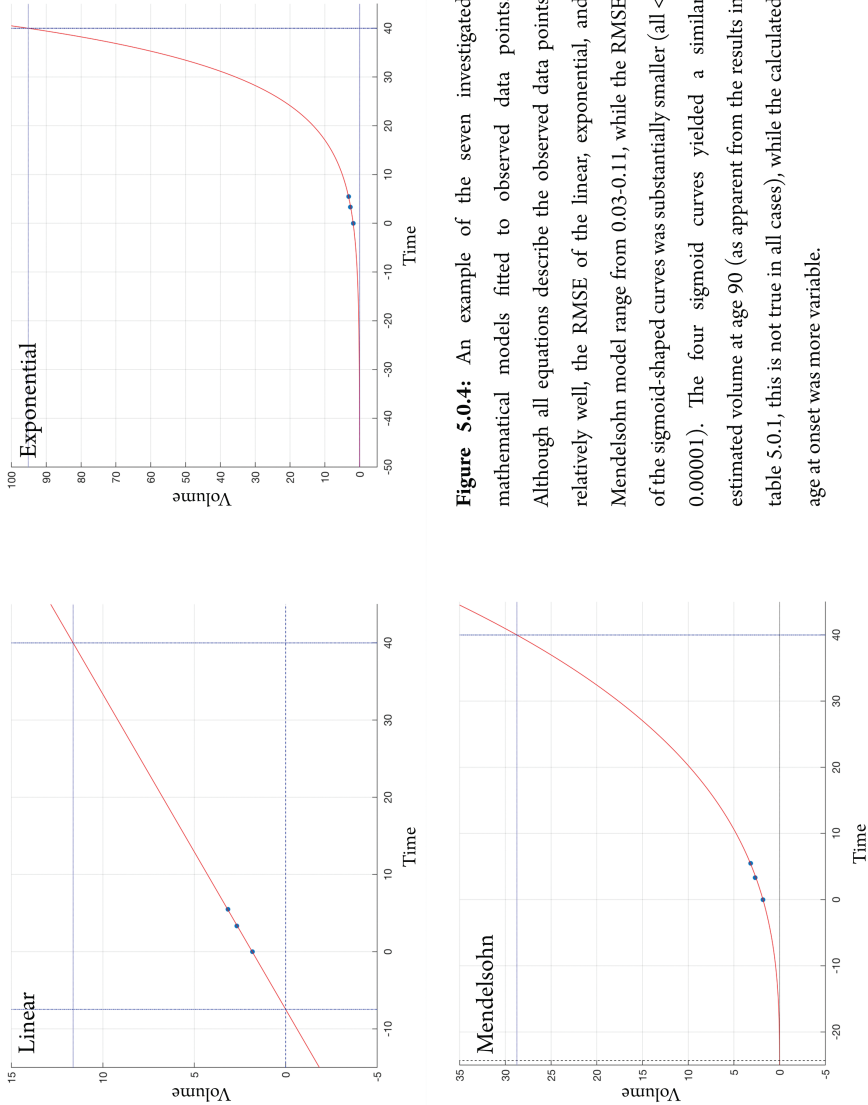


Figure 5.0.4: An example of the seven investigated mathematical models fitted to observed data points. Although all equations describe the observed data points relatively well, the RMSE of the linear, exponential, and Mendelsohn model range from 0.03-0.11, while the RMSE of the sigmoid-shaped curves was substantially smaller (all < 0.00001). The four sigmoid curves yielded a similar estimated volume at age 90 (as apparent from the results in table 5.0.1, this is not true in all cases), while the calculated age at onset was more variable.

DISCUSSION

Decelerating tumor growth laws, i.e., the Gompertz, logistic, Spratt, and Bertalanffy equations, were better suited to model growth of head and neck paragangliomas compared with the linear, exponential, or Mendelsohn models. This finding is in line with a previous observation of decreasing growth rates with increasing volume and age [9]. By definition, none of the investigated models could provide a perfect fit to alternating progression and regression as depicted in figure 5.0.2 d. However, as the smallest detectable difference was only exceeded in one of these cases, we propose growth, or rather the lack of it, was consistent with the plateau phase reached by all sigmoidal-shaped growth curves.

As stated by Vaidya et al, in addition to providing a good fit, a mathematical model should have a physiological basis [18]. Retardation of cell cycle speed was suggested as the mechanism behind the Gompertzian model [16]. However, this was contradicted by a more recently observed constant mitotic rate in renal cell carcinomas [11, 20]. Likewise, a solid physiological basis is lacking for the logistic, and Spratt models. Considering that the Bertalanffy equation is derived from basic cellular principles, we suggest this as an advantage over the other models, a proposal further reinforced by the observation that a realistic age at onset and volume at age 90 were generally predicted by the Bertalanffy model, while this was less clear in the Gompertz, logistic and Spratt models.

As most tumors are treated promptly following diagnosis, studies that use clinical images to model tumor growth are scarce. To the best of our knowledge, this is the first time that the Bertalanffy equation has been successfully fitted to clinically obtained growth data. In agreement with the current analysis, sigmoidal-shaped growth curves have been found to best describe growth of meningiomas and breast carcinomas [17, 21]. Evidence in favor of decelerating tumor growth is further provided by the observation of growth retardation with increasing age and volume, not only in paragangliomas but also in other benign and malignant tumors [22–25]. In fact, sigmoid curves were first used to model tumor growth, in view of the ever diminishing growth rate with increasing volume observed in animal models [11, 16]. Considering that the Gompertz, logistic, Spratt, and Bertalanffy models all fit our data almost equally well, we propose that the Bertalanffy model will also provide a good fit to growth data of tumors other than paragangliomas.

A minimum of three data points is required to model sigmoid-shaped growth curves. Therefore, tumors were only included if three consecutive MRI scans, before any intervention, were available. This may have resulted in a cohort with more favorable tumors, i.e., tumors that were left untreated after the second MRI. However, as the equations used are not restricted by growth rate, it is unlikely that the results are influenced by this potential bias.

Although we have not yet evaluated the accuracy of predictions, we believe we have made steps toward unraveling the natural course of head and neck paragangliomas. Neoplastic growth was estimated to commence in the third or fourth decade of life in most cases. However, dependent on the mathematical model used, neoplastic growth actually appeared to start prior to conception in a non-negligible number of cases. While this clearly indicates an imperfect fit, it probably indicates that neoplastic growth started very early in life in at least a few of these cases.

Following validation, mathematical models can, once three measurements are available, be used to differentiate between tumors that will probably cause serious symptoms and those that will likely remain asymptomatic. Subsequently, one can decide to switch to active treatment or continue conservative management.

Overdiagnosis, i.e., detection of occult disease that would have remained unnoticed throughout life, and subsequent overtreatment are not only associated with early detection of hereditary head and neck paragangliomas, but are intrinsic to cancer screening [26]. Although it is more or less possible to estimate the incidence of overdiagnosis at a population level, it is not as straightforward when it concerns individual patients [27, 28]. The benefits of screening, such as reduction of disease-specific morbidity and mortality, would be compromised if attempts were made to reduce overdiagnosis. However, by introducing conservative management strategies such as “watchful waiting”, harmful side effects of unnecessary treatment can be reduced. Perhaps the most well-known example is active surveillance for men with low-risk prostate cancer [29]. More recently, active surveillance was also introduced for clinical T1a renal lesions and low-risk ductal carcinoma in situ (DCIS) [30, 31]. We recognize that knowledge of tumor growth dynamics alone may not be sufficient to differentiate between aggressive and nonaggressive tumors, and additional criteria, including pathologic tumor features (e.g., Gleason upgrading in prostate cancer) or radiologic characteristics (e.g., increased density around calcifica-

tions of DCIS), will be required. However, we are now convinced that mathematical modeling of tumor growth is a useful determinant, as it provides not only the opportunity to estimate future tumor growth and thereby reduce overtreatment, but may also be used to estimate the age at onset and improve screening strategies.

CONCLUSION

Decelerating tumor growth laws best describe growth of carotid and vagal body paragangliomas. In addition, we have provided evidence that the often-neglected Bertalanffy equation can be used to model clinically obtained growth data and, in light of the generally realistic predicted age at onset of neoplastic growth and predicted volume at age 90, may even be the most appropriate mathematical model in this context. A better understanding of tumor growth dynamics will provide possibilities to optimize surveillance and reduce overtreatment.

REFERENCES

1. L. T. van Hulsteijn, B. Heesterman, J. C. Jansen, et al. "No evidence for increased mortality in SDHD variant carriers compared with the general population." In: *Eur. J. Hum. Genet.* 23.12 (2015), pp. 1713–6.
2. C. C. Boedeker. "Paragangliomas and paraganglioma syndromes." In: *GMS Curr. Top. Otorhinolaryngol. Head Neck Surg.* 10 (2011), Doc03.
3. J. L. Weissman and B. E. Hirsch. "Beyond the promontory: The multifocal origin of glomus tympanicum tumors." In: *Am. J. Neuroradiol.* 19.1 (1998), pp. 119–122.
4. C. C. Boedeker, E. F. Hensen, H. P. H. Neumann, et al. "Genetics of hereditary head and neck paragangliomas." In: *Head Neck* 36.6 (2014), pp. 907–16.
5. D. Taïeb, A. Kaliski, C. C. Boedeker, et al. "Current approaches and recent developments in the management of head and neck paragangliomas." In: *Endocr. Rev.* 35.5 (2014), pp. 795–819.
6. B. L. Heesterman, J. P. Bayley, C. M. Tops, et al. "High prevalence of occult paragangliomas in asymptomatic carriers of SDHD and SDHB gene mutations." In: *Eur. J. Hum. Genet.* 21.4 (2013), pp. 469–70.
7. C. Suárez, J. P. Rodrigo, W. M. Mendenhall, et al. "Carotid body paragangliomas: a systematic study on management with surgery and radiotherapy." In: *Eur. Arch. Otorhinolaryngol.* 271.1 (2014), pp. 23–34.
8. E. F. Hensen, J. C. Jansen, M. D. Siemers, et al. "The Dutch founder mutation SDHD.D92Y shows a reduced penetrance for the development of paragangliomas in a large multigenerational family." In: *Eur. J. Hum. Genet.* 18.1 (2010), pp. 62–66.
9. B. L. Heesterman, L. M. H. de Pont, B. M. Verbist, et al. "Age and tumor volume predict growth of carotid and vagal body paragangliomas." In: *J Neurol Surg B Skull Base* 78.6 (2017), pp. 497–505.
10. M. L. Carlson, A. D. Sweeney, G. B. Wanna, J. L. Netteville, and D. S. Haynes. "Natural History of Glomus Jugulare: A Review of 16 Tumors Managed with Primary Observation." In: *Otolaryngol. – Head Neck Surg.* 152.1 (2014), pp. 98–105.
11. P. Gerlee. "The model muddle: In search of tumor growth laws." In: *Cancer Res.* 73.8 (2013), pp. 2407–2411.
12. A. Talkington and R. Durrett. "Estimating Tumor Growth Rates In Vivo." In: *Bull. Math. Biol.* 77.10 (2015), pp. 1934–54.
13. S. Benzekry, C. Lamont, A. Beheshti, et al. "Classical mathematical models for description and prediction of experimental tumor growth." In: *PLoS Comput. Biol.* 10.8 (2014), e1003800.
14. B. L. Heesterman, B. M. Verbist, A. G. L. van der Mey, et al. "Measurement of head and neck paragangliomas: is volumetric analysis worth the effort? A method comparison study." In: *Clin. Otolaryngol.* 41.5 (2016), pp. 571–8.
15. V. P. Collins, R. K. Loeffler, and H. Tivey. "Observations on growth rates of human tumors." In: *Am. J. Roentgenol. Radium Ther. Nucl. Med.* 76.5 (1956), pp. 988–1000.
16. a. K. Laird. "Dynamics of Tumor Growth." In: *Br. J. Cancer* 13.1953 (1964), pp. 490–502.

17. J. A. Spratt, D. von Fournier, J. S. Spratt, and E. E. Weber. "Decelerating growth and human breast cancer." In: *Cancer* 71.6 (1993), pp. 2013–2019.
18. V. G. Vaidya and F. J. Alexandro. "Evaluation of some mathematical models for tumor growth." In: *Int J Biomed Comput* 13.1 (1982), pp. 19–36.
19. P. Som and H. Curtin. "Chapter 38 parapharyngeal and masticator space lesions." In: *Head neck imaging*. Ed. by P. Som and H. Curtin. 4th. Mosby, St. Louis, 2003, pp. 1954–2003.
20. W. T. Knöfel, U. Otto, H. Baisch, and G. Klöppel. "Stability of human renal cell carcinomas during long term serial transplantation into nude mice: histopathology, nuclear grade, mitotic rate, and DNA content in thirty tumors." In: *Cancer Res.* 47.1 (1987), pp. 221–4.
21. S. Nakasu, Y. Nakasu, T. Fukami, J. Jito, and K. Nozaki. "Growth curve analysis of asymptomatic and symptomatic meningiomas." In: *J. Neurooncol.* 102.2 (2011), pp. 303–310.
22. C. An, Y. A. Choi, D. Choi, et al. "Growth rate of early-stage hepatocellular carcinoma in patients with chronic liver disease." In: *Clin. Mol. Hepatol.* 21.3 (2015), pp. 279–286.
23. Y. Park, D. Choi, H. K. Lim, et al. "Growth rate of new hepatocellular carcinoma after percutaneous radiofrequency ablation: Evaluation with multiphase CT." In: *Am. J. Roentgenol.* 191.1 (2008), pp. 215–220.
24. P. L. Crispen, A. Soljic, G. Stewart, A. Kutikov, D. Davenport, and R. G. Uzzo. "Enhancing renal tumors in patients with prior normal abdominal imaging: Further insight into the natural history of renal cell carcinoma." In: *J. Urol.* 188.4 (2012), pp. 1089–1093.
25. J. Honegger, S. Zimmermann, T. Psaras, et al. "Growth modelling of non-functioning pituitary adenomas in patients referred for surgery." In: *Eur. J. Endocrinol.* 158.3 (2008), pp. 287–294.
26. M. Jung. "Breast, prostate, and thyroid cancer screening tests and overdiagnosis." In: *Curr. Probl. Cancer* 41.1 (2016), pp. 71–79.
27. G. Draisma, R. Etzioni, A. Tsodikov, et al. "Lead time and overdiagnosis in prostate-specific antigen screening: Importance of methods and context." In: *J. Natl. Cancer Inst.* 101.6 (2009), pp. 374–383.
28. J. R. Benson, I. Jatoi, and M. Toi. "Treatment of low-risk ductal carcinoma in situ: is nothing better than something?" In: *Lancet. Oncol.* 17.10 (2016), e442–e451.
29. L. P. Bokhorst, R. Valdagni, A. Rannikko, et al. "A Decade of Active Surveillance in the PRIAS Study: An Update and Evaluation of the Criteria Used to Recommend a Switch to Active Treatment." In: *Eur. Urol.* 70.6 (2016), pp. 954–960.
30. L. E. Elshof, K. Tryfonidis, L. Slaets, et al. "Feasibility of a prospective, randomised, open-label, international multicentre, phase III, non-inferiority trial to assess the safety of active surveillance for low risk ductal carcinoma in situ - The LORD study." In: *Eur. J. Cancer* 51.12 (2015), pp. 1497–1510.
31. M. Nayyar, P. Cheng, B. Desai, et al. "Active Surveillance of Small Renal Masses: A Review on the Role of Imaging With a Focus on Growth Rate." In: *J. Comput. Assist. Tomogr.* 40.4 (2016), pp. 517–23.